

Article

# The Effect of Unbalanced Impedance Loads on the Short-Circuit Current

Insu Kim 

School of Electrical Engineering, Inha University, Incheon 22212, Korea; insu@inha.ac.kr; Tel.: +82-32-860-7395

Received: 23 March 2018; Accepted: 27 April 2018; Published: 4 June 2018



**Abstract:** Conventional short-circuit studies often neglect the load current because the short-circuit current (SCC) flowing from generators is much greater than the SCC that is affected by various loading conditions. As distributed or clustered loads that are unbalanced in phases are connected to the grid, they can also change the magnitude and phase angle of the SCC, despite their small capacities. Thus, the objective of this study is to present algorithms that are able to analyze such an impedance unbalanced load. For this purpose, this study initially derives an SCC model of the unbalanced impedance load in phases. Since the proposed SCC model requires the pre-fault voltage, it uses a power-flow analysis algorithm that iteratively calculates the current that is to be injected and the pre-fault voltage, using the bus impedance matrix. Then, the proposed SCC calculation algorithm transforms the unbalanced loads into equivalent impedances, using the pre-fault voltage, and adds them to sequence networks as input data, using the proposed SCC model. The proposed algorithms are verified in various case studies. As a result, the proposed SCC calculation algorithms are more accurate, because they do not neglect unbalanced loads.

**Keywords:** bus impedance matrix; iterative current compensation; sequence network; short-circuit current (SCC) model; unbalanced delta-connected load; unbalanced wye-connected load

## 1. Introduction

The load current in short-circuit studies is often neglected because the magnitude of the short-circuit current (SCC) flowing from rotating generators is much greater than the magnitude of the SCC that is affected by loads. As distributed or clustered loads that are unbalanced in phases are connected to the grid, they can significantly change the magnitude and phase angle of the SCC, despite their small capacities. Thus, the load current should not be neglected in short-circuit studies. Therefore, many studies have presented various methods for calculating the SCC. For example, in [1], the equivalent circuits of a faulted network, which includes renewable energy sources based on voltage source converters, are proposed. The SCC problem is also solved by the iterative current compensation method with the bus impedance matrix [2]. Since the topology of the distribution system is usually either radial or weakly meshed, the Thevenin equivalent circuit is also solved by the backward and forward sweep (BFSW) method [3]. To synthesize the stochastic variation in the SCC, in [4], the probabilistic simulations (e.g., Monte Carlo simulations) are performed. In [5,6], the decomposition method of the bus impedance matrices to bus-current-injection to branch-current (BIBC), and branch-current to bus-voltage (BCBV) matrices, which were originally proposed for power-flow calculation, are also applied to the SCC calculation. Moreover, to apply the SCC calculation algorithm to the real-time system, a hybrid compensation method that uses the Thevenin equivalent impedance matrix, based on phase representation, is presented in [7].

While the previous studies are based on balanced three-phase systems, the SCC of the multi-phase distribution systems is calculated by representing the multi-phase distribution system as the equivalent three-phase system in [8]. Similarly, when an internal fault occurs in the twelve-phase transmission

lines, the faulted voltages and currents are also decomposed into twelve-sequence components (e.g., positive-sequence currents and inverted sequence components) that take the effect of the mutual coupling of the twelve-phase lines on the SCC into account, so that the proposed method can find the fault location [9]. Since the previous studies do not examine the series and simultaneous faults, a generic SCC model, which uses Thevenin's voltage, impedance, and fault network models that are able to analyze the series and simultaneous faults, is presented in three-phase coordinates [10]. Furthermore, the  $n$ -conductor current injection method (NCIM) that solves the non-linear equations and calculates the state variables (e.g., the line currents and phase-to-ground voltages), based on the Newton–Raphson method, is proposed in [11]. The  $n$ -conductor fault method also analyzes the internal, series, and simultaneous faults, based on the extended version of the NCIM [12].

Meanwhile, although the previous studies provide various SCC calculation methods, they do not focus on heavily unbalanced distribution systems. Thus, in [13], the augmented nodal matrix, which has been selected by the inversion technique, solves the SCC problem of unbalanced distribution systems, including the independent voltage sources, transformer models, and switches. The coupling relationship between the sequence networks of three- and six-phase lines are derived in [14]. Then, using the augmented admittance matrices, a part that has been selected from the admittance matrix—the unbalance in a network that includes three- and six-phase systems that are caused by untransposed lines and transformer phase shifts (e.g.,  $\pm 30^\circ$  in a delta-wye)—is also examined in [14]. For multiple faults on the unbalanced poly-phase systems, using nodal impedance and admittance matrices, the phase coordinate representation of the system is also derived in [15]. Additionally, for a transient stability study of the unbalanced conditions after faults, the positive-sequence admittance matrix, which represents the relationship between generators and dynamic loads, is derived in [16].

The previous studies neglect the system unbalance that is caused by inverter-based distributed generation (IBDG) sources, so after assuming that the IBDG source operates at a power factor (PF) of 1.0 or 0, the contribution of such an IBDG source to the SCC is examined by solving Kirchhoff's current law (KCL) equations using the Newton-Raphson method [17]. To calculate an SCC of the unbalanced microgrid with microturbine generators, branch mismatch currents are injected and mismatch voltages are calculated using the relationship between the BIBC and BCBV matrices [18]. To estimate the fault impedance and SCC in unbalanced and untransposed feeders, the study [19], assumes that two voltage sources are connected in series. The first voltage source corresponds to the pre-fault voltage and the second source represents the fault type boundary conditions.

However, these previous short-circuit studies have neglected the load current for the following reasons.

- (1) The SCC that is changed in the loading conditions is much smaller than the SCC that neglects loads.
- (2) The loads that are operated in modern power grids can not be modeled by 'simple' impedance during an electric fault [20].

However, recently, in [21], loads that are connected in wye or delta are modeled as constant impedances and their contribution to the SCC is calculated by not only combining the network and the faulted side, but also by converting the faulted side into equivalent injected current sources, using the three-phase impedance matrix. The loads that are unbalanced in either radial or weakly meshed distributions (the IEEE 123-bus test feeder) are also modeled as constant impedances and are added to the bus admittance matrix. Then, the study compares the cases of loaded and unloaded conditions [22]. Moreover, in order to take the load current into account, one study proposes a method that removes the system frequency variations from a set of phasors that are measured by phasor measurement units, and estimates the SCC in varying load conditions [23]. Another study also presents an SCC identification algorithm that forecasts the short-term load and extrapolates the grid state, based on neural networks [24]. While the previous studies ignore dynamic loads, the effect of dynamic loads on the SCC is examined by PSS/E simulations [25]. The effect of the dynamic loads on the three-phase SCC of metropolitan transmission networks is also studied by comparing the digital fault recorder data and

PSS/E simulation data [26]. Recently, a method that transforms the delta- and wye-connected loads that are balanced in three phases to the equivalent impedances, and adds them to the conventional sequence network, is presented in [27,28].

In the meantime, many short-circuit studies have used power systems computer analysis programs, including CYME, DIgSILENT, PSS/E, and SIMULINK of MATLAB. However, although the programs provide an SCC calculation mode that takes the load current into account, they replace Thevenin's voltage in the positive-sequence network with the pre-fault voltage that is determined by their power-flow calculation function when calculating the SCCs [29,30]. Furthermore, they do not present the detailed modeling equations of the SCC that are affected by the load current in their manual [29,30].

The previous studies that are mentioned above have neglected the unbalanced wye- or delta-connected loads when calculating the SCC. Therefore, this study derives the equivalent short-circuit models of the wye- or delta-connected unbalanced loads in single or two phases, and adds the equivalent short-circuit models to the positive-, negative-, and zero-sequence networks. In fact, the proposed equivalent model uses the pre-fault voltage for more accurately calculating the SCC, so a power-flow calculation algorithm is also presented. The power-flow calculation method, which is proposed in [31,32], significantly reduces the inversion of the matrices, so it is faster than the conventional power-flow calculation methods (e.g., the Gauss–Seidel, Newton–Raphson, and fast decoupled methods) for a large-sized power grid (e.g., with thousands of nodes). However, the methods that are presented in [31,32], do not include tap-changing transformers and P-V buses. Therefore, this study proposes decomposing the system into the series and shunt components in order to model tap-changing transformers. The detailed modeling methods of P-V buses and tap-changing transformers will be presented in Part II of this paper. In addition to the faster speed, the proposed SCC models calculate the SCC more accurately, by not ignoring the wye- or delta-connected unbalanced loads in single or two phases, which is verified in various case studies by comparing the cases of (a) neglecting loads, (b) converting loads to impedance using the nominal voltage, and (c) the actual SCC.

This study is presented in the following sections. Section 2 derives the equivalent short-circuit models of the unbalanced impedance loads. Section 3 briefly introduces the pre-fault voltage calculation method that uses the bus impedance matrix and the iterative current compensation method. Section 4 presents case studies that validate the proposed methods. Section 5 summarizes the main conclusions of this study.

## 2. Short-Circuit Current Model

A distribution system is usually neither balanced nor fully transposed. To the best of our knowledge, none of the previous studies have derived an SCC model of the unbalanced wye- or delta-connected loads, so this study proposes the following equivalent short-circuit models of such an unbalanced load. The proposed SCC model is based on an unbalanced network. Thus, it is applicable to either an unbalanced or untransposed system.

### 2.1. Unbalanced Loads

#### 2.1.1. Delta-Connected Unbalanced Impedance Loads

A delta-connected unbalanced impedance load is connected to between phases *A* and *B*, in Figure 1. Each line-to-line voltage is as follows:

$$\begin{bmatrix} V_{AB} \\ V_{BC} \\ V_{CA} \end{bmatrix} = \begin{bmatrix} V_A - V_B \\ V_B - V_C \\ V_C - V_A \end{bmatrix} = \mathbf{V}_{ABC} - \begin{bmatrix} 0 & 1 & 0 \\ 0 & 0 & 1 \\ 1 & 0 & 0 \end{bmatrix} \mathbf{V}_{ABC} = \begin{bmatrix} I_A Z_{AB} \\ 0 \\ 0 \end{bmatrix}. \quad (1)$$

If applying  $\mathbf{V}_{ABC} = \mathbf{A}\mathbf{V}_{012}$  to (1), the sequence voltage is:

$$\mathbf{A}\mathbf{V}_{012} - \begin{bmatrix} 0 & 1 & 0 \\ 0 & 0 & 1 \\ 1 & 0 & 0 \end{bmatrix} \mathbf{A}\mathbf{V}_{012} = \begin{bmatrix} I_A Z_{AB} \\ 0 \\ 0 \end{bmatrix} \tag{2}$$

If multiplying  $\mathbf{A}^{-1}$  to each side, the sequence voltage is as follows:

$$\mathbf{V}_{012} = \mathbf{A}^{-1} \begin{bmatrix} 0 & 1 & 0 \\ 0 & 0 & 1 \\ 1 & 0 & 0 \end{bmatrix} \mathbf{A}\mathbf{V}_{012} + \mathbf{A}^{-1} \begin{bmatrix} I_A Z_{AB} \\ 0 \\ 0 \end{bmatrix} = \begin{bmatrix} 1 & 0 & 0 \\ 0 & 1\angle 240^\circ & 0 \\ 0 & 0 & 1\angle 120^\circ \end{bmatrix} \mathbf{V}_{012} + \mathbf{A}^{-1} \begin{bmatrix} I_A Z_{AB} \\ 0 \\ 0 \end{bmatrix}. \tag{3}$$

The positive- and negative-sequence components of (3) are as follows:

$$\begin{bmatrix} V_1 - 1\angle 240^\circ V_1 \\ V_2 - 1\angle 120^\circ V_2 \end{bmatrix} = \begin{bmatrix} (1 - 1\angle 240^\circ)V_1 \\ (1 - 1\angle 120^\circ)V_2 \end{bmatrix} = \frac{I_A Z_{AB}}{3} \begin{bmatrix} 1 \\ 1 \end{bmatrix}. \tag{4}$$

The sequence component of the line current is as follows:

$$\mathbf{I}_{012} = \mathbf{A}^{-1} \begin{bmatrix} I_A \\ I_B \\ I_C \end{bmatrix} = \mathbf{A}^{-1} \begin{bmatrix} I_A \\ -I_A \\ 0 \end{bmatrix} = \frac{I_A}{3} \begin{bmatrix} 0 \\ 1 - 1\angle 120^\circ \\ 1 - 1\angle 240^\circ \end{bmatrix}. \tag{5}$$

Combining Equations (4) and (5) yields the following:

$$\begin{bmatrix} I_0 \\ I_1 \\ I_2 \end{bmatrix} = \begin{bmatrix} 0 \\ V_1 \\ V_2 \end{bmatrix} / \frac{Z_{AB}}{3}. \tag{6}$$

Equation (6) is represented by the positive-, negative-, and zero-sequence networks in Figure 2.

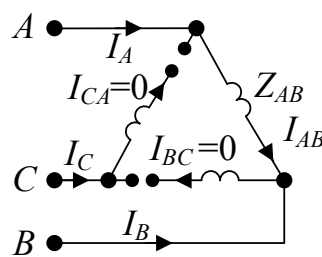


Figure 1. A delta-connected impedance load unbalanced in two phases.  $V$ —voltage;  $Z$ —impedance.

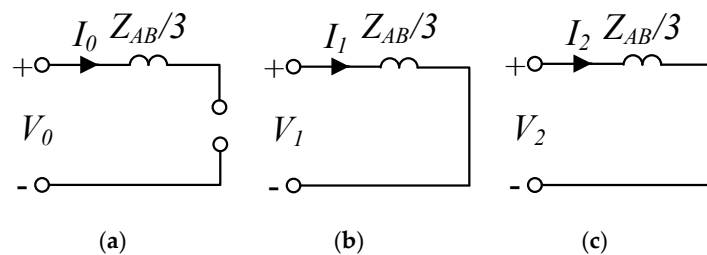


Figure 2. The unbalanced delta-connected impedance load decomposed into the sequence model: (a) zero sequence; (b) positive sequence; and (c) negative sequence.

### 2.1.2. Wye-Connected Unbalanced Impedance Loads

A wye-connected single-phase impedance load is connected to between phases *A* and *N*, in Figure 3. Each phase voltage is as follows:

$$\mathbf{V}_{ABC} = I_A \begin{bmatrix} (Z_A + Z_N) \\ Z_N \\ Z_N \end{bmatrix} = \mathbf{A}\mathbf{V}_{012}, \tag{7}$$

where  $\mathbf{A} = [1 \ 1 \ 1; 1 \angle 240^\circ \ 1 \angle 120^\circ; 1 \angle 120^\circ \ 1 \angle 240^\circ]$ .

The sequence voltage is as follows:

$$\mathbf{V}_{012} = \mathbf{A}^{-1}I_A \begin{bmatrix} (Z_A + Z_N) \\ Z_N \\ Z_N \end{bmatrix} = \frac{I_A}{3} \begin{bmatrix} (Z_A + 3Z_N) \\ Z_A \\ Z_A \end{bmatrix}. \tag{8}$$

The sequence current is as follows:

$$\mathbf{I}_{012} = \mathbf{A}^{-1} \begin{bmatrix} I_A \\ I_B \\ I_C \end{bmatrix} = \mathbf{A}^{-1} \begin{bmatrix} I_A \\ 0 \\ 0 \end{bmatrix} = \frac{I_A}{3} \begin{bmatrix} 1 \\ 1 \\ 1 \end{bmatrix}. \tag{9}$$

Combining Equations (8) and (9) yields the following:

$$\mathbf{V}_{012} = \frac{I_A}{3} \begin{bmatrix} (Z_A + 3Z_N) \\ Z_A \\ Z_A \end{bmatrix} = \begin{bmatrix} (Z_A + 3Z_N)I_0 \\ Z_A I_1 \\ Z_A I_2 \end{bmatrix}. \tag{10}$$

Equation (10) is represented by the positive-, negative-, and zero-sequence networks in Figure 4.

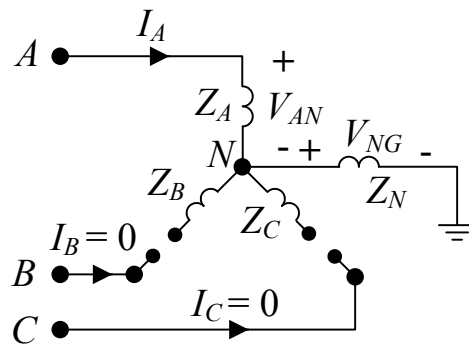


**Figure 3.** A wye-connected impedance load unbalanced in a single phase.

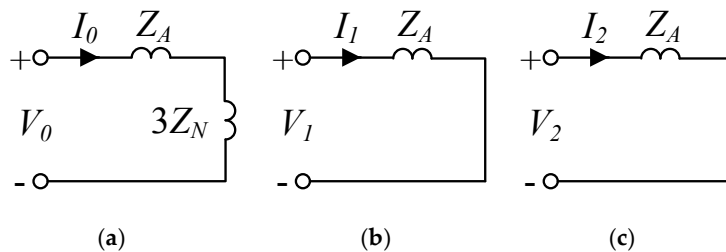


**Figure 4.** The unbalanced wye-connected impedance load decomposed into the sequence model: (a) zero sequence; (b) positive sequence; and (c) negative sequence.

If an unbalanced wye- or delta-connected impedance load is connected to other phases (e.g.,  $B-N$ ,  $C-N$ ,  $B-C$ , or  $C-A$ ), the equivalent model in Figures 2 and 4 can be replaced by the corresponding impedance that is connected to other phases. The conventional short-circuit studies have often ignored the load currents, because the magnitude of the SCC is higher than the magnitude of the load current. However, the proposed method transforms the unbalanced impedance loads to the equivalent SCC models and adds them to each sequence network, so that it can calculate the SCC more accurately. That is, it can take the effect of unbalanced loads on the SCC into account. However, the proposed unbalanced load model is only valid for the impedance loads. To take other load types (e.g., constant current and power load types) into account, the following approximation method is also used.

### 2.2. Transformation of Constant Current and Power Loads to Equivalent Impedance

The current that is flows to the constant power and current loads at the nominal voltage can be close to the current that is flows to constant impedance loads. Furthermore, the rated capacity of the constant power and current loads is often specified by active and reactive power in kVA or MVA. Thus, the constant power and current loads can be approximated by the constant impedance load in short-circuit analyses [21,22,27].

$$Z = \frac{\tilde{V}}{\tilde{I}} = \frac{\tilde{V}}{\left(\frac{S}{\tilde{V}}\right)^*} = \frac{V^2}{S^*}, \quad (11)$$

where  $V$  = the pre-fault voltage in per unit (p.u.), and  $S$  = the complex power scheduled at the load in p.u.

However, since the voltage of the unbalanced loads during a fault is usually different from the pre-fault voltage, the proposed approximation has inherent errors to the actual SCC. Thus, this study compares the SCC that is approximated by the proposed method to the SCC that is calculated by the following superposition rule.

### 2.3. Superposition

The voltage of the faulted bus ( $V_f$ ) in the SCC equations, presented in Table A1 of the Appendix A, is often assumed as  $1\angle 0^\circ$  p.u. If ignoring the load in Figure 5, the SCC ( $I_{f,no-load}$ ) is as follows:

$$I_{f,no-load} = \frac{V_s}{z_i}. \quad (12)$$

The load current before the fault is as follows:

$$I_{load} = \frac{V_s}{z_i + z_j + z}. \quad (13)$$

As a result of the assumption of  $V_f$  (e.g.,  $1\angle 0^\circ$  p.u.), the bus voltage at the slack generator should be increased by the following:

$$V_{s,loading} = V_s + z_i I_{load}. \quad (14)$$

Thus, the actual SCC that takes the load current into account can be determined by the following superposition rule:

$$I_{fault} = \frac{V_{s,loading}}{z_i} = \frac{V_s + z_i I_{load}}{z_i} = I_{f,no-load} + I_{load}. \quad (15)$$

Note that the superposition rule based on Equation (15) can be applied for line-to-line (LL), line-to-line ground (LLG), and three-phase faults.

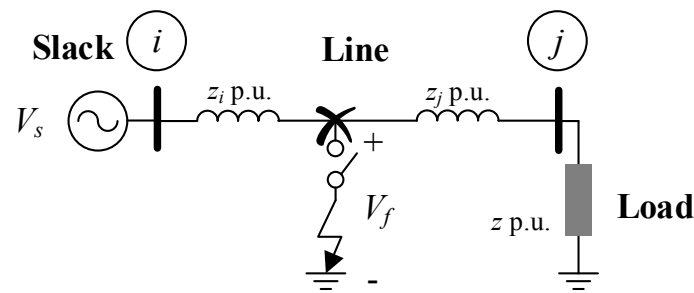


Figure 5. An example of the superposition rule; p.u.—per unit;  $V_f$ —faulted bus voltage.

### 3. Pre-Fault Voltage Calculation

The proposed equivalent SCC model required the pre-fault voltage in order to more accurately calculate the SCC, so a power-flow calculation algorithm was presented in [31,32]. The method represented the power system network as the bus impedance matrix, or  $\mathbf{Z}_{bus}$ , and then calculated the power flow without any further processing of the impedance matrix. Indeed,  $\mathbf{Z}_{bus}$  represented the relationship between the injected currents and the induced voltages by the following:

$$\mathbf{V} = \mathbf{Z}_{bus}\mathbf{I}. \quad (16)$$

To build the bus impedance matrix, in Figure 6, this study introduced the following four rules:

(1) *The slack node needed to be connected to the reference (e.g., the ground).* If a slack node was connected to the reference, the initial  $Z_{bus}$  is built by the following:

$$\mathbf{Z}_{bus}^{(1)} = [0.1j] \text{ p.u.} \quad (17)$$

(2) *The new nodes needed to be connected to the slack node.* If the new node  $j$ , with an impedance of  $z$  p.u., was connected to the previous node  $i$ , the following rule is used:

$$\mathbf{Z}_{bus}^{(v)} = \begin{bmatrix} \mathbf{Z}_{bus}^{(v-1)} & \mathbf{Z}_i^{(v-1)} \\ (\mathbf{Z}_i^{(v-1)})^T & \mathbf{Z}_{ii}^{(v-1)} + z \end{bmatrix}, \quad (18)$$

where  $\mathbf{Z}_{bus}^{(v)}$  and  $\mathbf{Z}_{bus}^{(v-1)} = Z_{bus}$  at the new and previous steps, respectively;

$\mathbf{Z}_i^{(v-1)}$  = the  $i$ th column vector of the previous step;

and  $\mathbf{Z}_{ii}^{(v-1)}$  = the element of the  $i$ th row and  $i$ th column, at the previous step.

For example, if the new nodes 2 and 3, in Figure 6, were connected to the slack bus (e.g., node 1),  $Z_{bus}$  was modified by the following:

$$\mathbf{Z}_{bus}^{(2)} = \begin{bmatrix} 0.1j & 0.1j \\ 0.1j & 0.3i \end{bmatrix} \text{ p.u.}, \mathbf{Z}_{bus}^{(3)} = \begin{bmatrix} 0.1j & 0.1j & 0.1j \\ 0.1j & 0.3i & 0.3j \\ 0.1j & 0.3j & 0.6j \end{bmatrix} \text{ p.u.} \quad (19)$$

(3) *The new node needed to be connected to the existing two nodes.* If the new node, with an impedance of  $z$  p.u., was connected to the existing two nodes (e.g., nodes  $i$  and  $j$ ), the following rule modified the existing  $Z_{bus}$ :

$$\mathbf{Z}_{bus}^{(v)} = \mathbf{Z}_{bus}^{(v-1)} - (z + \frac{1}{z_{ii}^{(v-1)}} + \frac{1}{z_{jj}^{(v-1)}} - 2\frac{1}{z_{ij}^{(v-1)}})^{-1} (\frac{1}{z_{ii}^{(v-1)}} - \frac{1}{z_{jj}^{(v-1)}}) (\frac{1}{z_{ii}^{(v-1)}} - \frac{1}{z_{jj}^{(v-1)}})^T. \quad (20)$$

For example, if a new node, with an impedance of  $0.4j$  p.u., was connected to the existing nodes (e.g., nodes 1 and 3, thus  $i = 1$  and  $j = 3$ ),  $Z_{bus}$  was modified by the following:

$$\mathbf{Z}_{bus}^{(v)} = \begin{bmatrix} 0.1j & 0.1j & 0.1j \\ 0.1j & 0.2556j & 0.1889j \\ 0.1j & 0.1889j & 0.3222j \end{bmatrix} \text{ p.u.} \quad (21)$$

(4) *The Kron reduction of the existing node.* If the existing node was connected to the reference through an impedance of  $z$  p.u., the following Kron reduction rule was used:

$$\mathbf{Z}_{ij}^{(v)} = \mathbf{Z}_{ij}^{(v-1)} - \frac{\mathbf{Z}_{in}^{(v-1)}\mathbf{Z}_{nj}^{(v-1)}}{\mathbf{Z}_{nn}^{(v-1)} + z}, \quad (22)$$

where  $n$  = the node connected to the reference,  $i$  and  $j = 1, \dots, n$ .

If the existing node (e.g.,  $n = 3$ ) was connected to the reference, through an impedance of  $0.1j$  p.u., final  $Z_{bus}$  is as follows:

$$\mathbf{Z}_{bus}^{(v)} = \begin{bmatrix} 0.0763j & 0.0553j & 0.0237j \\ 0.0553j & 0.1711j & 0.0447j \\ 0.0237j & 0.0447j & 0.0763j \end{bmatrix} \text{ p.u.} \quad (23)$$

These four rules built the bus impedance matrices that calculated the power flow and SCC of the positive-, negative-, and zero-sequence networks of the test feeders.

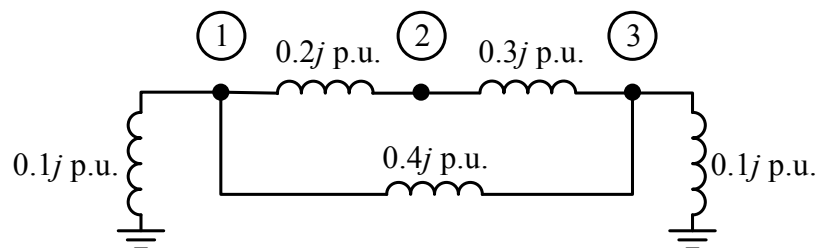


Figure 6. A power grid example with three nodes.

The method presented in [31,32] calculated the currents that were to be injected and the voltages that were induced by the currents. If the actual pre-fault voltages were known at the first iteration, the method could determine the actual currents. But, the pre-fault voltages that were estimated at the first step were based on the initial nominal voltages. Thus, the steps that determined the injected currents and the induced voltages, or Equation (16), were iterated until they achieved the convergence in the following mismatch:

$$\Delta V_j^{(k)} = \left| \tilde{V}_j^{(k)} - \tilde{V}_j^{(k-1)} \right| \leq \varepsilon. \quad (24)$$

However, the method presented in [31,32] did not model the tap-changing transformers and P-V buses. Therefore, this study decomposed the system into the series and shunt components, in order to model the tap-changing transformers. The detailed modeling methods of P-V buses and tap-changing transformers were done beyond this study, so they will be presented in Part II of this paper.

## 4. Case Studies

### 4.1. Seven-Bus Radial System

To verify the proposed iterative bus impedance method that was able to calculate not only the power flow in the normal steady state, but also the SCC that was affected by loads, a distribution system with unbalanced loads and a distributed generation (DG) source is modeled in Figure 7. The system



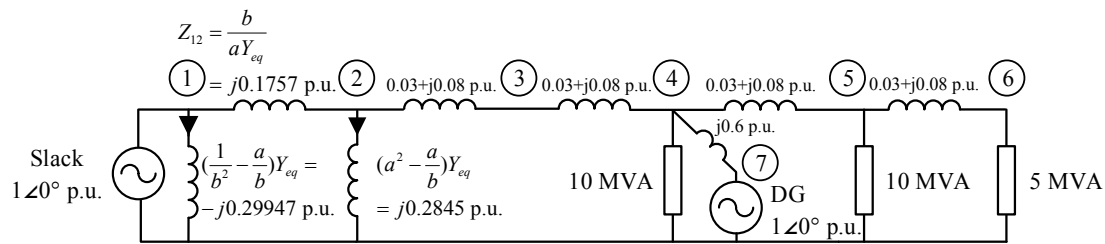


**Figure 8.** A single-phase network diagram of the test system at a base of 100 MVA (all values in per unit [p.u.]).

The method iteratively calculated the injected currents and induced voltages, using the matrices (e.g., Equations (25) and (26)) until the convergence was achieved. This study compared the power-flow calculation results to the verified methods (e.g., the Newton–Raphson, Gauss–Seidel, and fast decoupled methods), in Table 1. The proposed method showed the same exact pre-fault voltages as those that were determined by the other methods, and successfully modeled the tap-changing transformer with an off-nominal tap ratio, which could be seen in the voltage of bus 2 (e.g.,  $1.03446 \angle -1.528^\circ$  p.u.). Thus, the pre-fault voltage could be used in the proposed SCC model, which transformed the load to the equivalent impedance in Equation (11).

**Table 1.** Positive-sequence pre-fault voltage and generation in per unit (p.u.); V—voltage.

Bus		Proposed Method	Newton-Raphson	Gauss-Seidel	Fast Decoupled
1	V	$1.00000 \angle 0.000^\circ$	$1.00000 \angle 0.000^\circ$	$1.00000 \angle 0.000^\circ$	$1.00000 \angle 0.000^\circ$
	Generation	$0.157 + 0.105j$	$0.157 + 0.105j$	$0.157 + 0.105j$	$0.157 + 0.105j$
2	V	$1.03446 \angle -1.528^\circ$	$1.03446 \angle -1.528^\circ$	$1.03446 \angle -1.528^\circ$	$1.03446 \angle -1.528^\circ$
3	V	$1.02226 \angle -2.047^\circ$	$1.02226 \angle -2.047^\circ$	$1.02226 \angle -2.047^\circ$	$1.02226 \angle -2.047^\circ$
4	V	$1.01014 \angle -2.578^\circ$	$1.01014 \angle -2.578^\circ$	$1.01014 \angle -2.578^\circ$	$1.01014 \angle -2.578^\circ$
	Load	$0.100 + j0.000$	$0.100 + j0.000$	$0.100 + j0.000$	$0.100 + j0.000$
5	V	$1.00030 \angle -3.042^\circ$	$1.00030 \angle -3.042^\circ$	$1.00030 \angle -3.042^\circ$	$1.00030 \angle -3.042^\circ$
	Load	$0.090 + j0.044$	$0.090 + j0.044$	$0.090 + j0.044$	$0.090 + j0.044$
6	V	$0.99669 \angle -3.175^\circ$	$0.99669 \angle -3.175^\circ$	$0.99669 \angle -3.175^\circ$	$0.99669 \angle -3.175^\circ$
	Load	$0.040 + j0.030$	$0.040 + j0.030$	$0.040 + j0.030$	$0.040 + j0.030$
7	V	$1.00000 \angle 0.000^\circ$	$1.00000 \angle 0.000^\circ$	$1.00000 \angle 0.000^\circ$	$1.00000 \angle 0.000^\circ$
	Generation	$0.076 - 0.015j$	$0.076 - 0.015j$	$0.076 - 0.015j$	$0.076 - 0.015j$

#### 4.1.2. Short-Circuit Current Calculation

To determine the SCC of the proposed case study, this study applied the pre-fault voltage of a bus (to which the loads were connected) to Equations (6), (10), and (11). In other words, the first two loads that were connected in a wye were transformed to the equivalent impedance by the following:

$$Z_{B4}^Y = \frac{V_{B4}^2}{S_{B4}^*} = \frac{1.01014^2}{(0.1 + 0j)^*} = 10.2037 \text{ p.u.} \quad (27)$$

$$Z_{B5}^Y = \frac{V_{B5}^2}{S_{B5}^*} = \frac{1.00030^2}{(0.09 + 0.04359j)^*} = 9.0054 + 4.3615j \text{ p.u.} \quad (28)$$

The third load that was connected in a delta was transformed to the equivalent impedance by the following:

$$Z_{B6}^\Delta = \frac{V_{B6}^2}{3S_{B6}^*} = \frac{0.99669^2}{3(0.04 + 0.03j)^*} = 5.2980 + 3.9735j \text{ p.u.} \quad (29)$$

Using the proposed SCC models of Equations (6) and (10), the equivalent impedances were added to the positive-, negative-, and zero-sequence networks, in Figure 9. Note that the third load that was connected in a delta was an open circuit in the zero-sequence network, according to the proposed SCC model in Equation (6). Figure 9 shows the sequence networks that were connected in series after the occurrence of a single line-to-ground (SLG) fault on bus 3 of the test system. Then, this study built the impedance matrix of each sequence network by the following:

$$Z_{bus}^+ = Z_{bus}^- = \begin{bmatrix} 0.0000 + 0.0000i & 0.0000 + 0.0000i \\ 0.0000 + 0.0000i & 0.0064 + 0.1474i & 0.0031 + 0.1301i & -0.0003 + 0.1128i & 0.0011 + 0.1109i & 0.0019 + 0.1097i & 0.0000 + 0.0000i & 0.0000 + 0.0000i \\ 0.0000 + 0.0000i & 0.0031 + 0.1301i & 0.0255 + 0.1859i & 0.0179 + 0.1617i & 0.0196 + 0.1587i & 0.0205 + 0.1569i & 0.0000 + 0.0000i & 0.0000 + 0.0000i \\ 0.0000 + 0.0000i & -0.0003 + 0.1128i & 0.0179 + 0.1617i & 0.0361 + 0.2105i & 0.0381 + 0.2065i & 0.0391 + 0.2040i & 0.0000 + 0.0000i & 0.0000 + 0.0000i \\ 0.0000 + 0.0000i & 0.0011 + 0.1109i & 0.0196 + 0.1587i & 0.0381 + 0.2065i & 0.0704 + 0.2809i & 0.0716 + 0.2774i & 0.0000 + 0.0000i & 0.0000 + 0.0000i \\ 0.0000 + 0.0000i & 0.0019 + 0.1097i & 0.0205 + 0.1569i & 0.0381 + 0.2065i & 0.0716 + 0.2774i & 0.1029 + 0.3528i & 0.0000 + 0.0000i & 0.0000 + 0.0000i \\ 0.0000 + 0.0000i & 0.0000 + 0.0000i \end{bmatrix} \text{ p.u.} \quad (30)$$

$$Z_{bus}^0 = \begin{bmatrix} 0.0000 + 0.0000i & 0.0000 + 0.0000i \\ 0.0000 + 0.0000i & 0.0077 + 0.2155i & 0.0032 + 0.1752i & -0.0014 + 0.1349i & 0.0004 + 0.1334i & 0.0004 + 0.1334i & 0.0000 + 0.0000i & 0.0000 + 0.0000i \\ 0.0000 + 0.0000i & 0.0032 + 0.1752i & 0.0301 + 0.2811i & 0.0170 + 0.2170i & 0.0197 + 0.2143i & 0.0197 + 0.2143i & 0.0000 + 0.0000i & 0.0000 + 0.0000i \\ 0.0000 + 0.0000i & -0.0014 + 0.1349i & 0.0170 + 0.2170i & 0.0355 + 0.2991i & 0.0390 + 0.2953i & 0.0390 + 0.2953i & 0.0000 + 0.0000i & 0.0000 + 0.0000i \\ 0.0000 + 0.0000i & 0.0004 + 0.1334i & 0.0197 + 0.2143i & 0.0390 + 0.2953i & 0.0843 + 0.4591i & 0.0843 + 0.4591i & 0.0000 + 0.0000i & 0.0000 + 0.0000i \\ 0.0000 + 0.0000i & 0.0004 + 0.1334i & 0.0197 + 0.2143i & 0.0390 + 0.2953i & 0.0843 + 0.4591i & 0.0843 + 0.4591i & 0.0000 + 0.0000i & 0.0000 + 0.0000i \\ 0.0000 + 0.0000i & 0.0000 + 0.0000i \end{bmatrix} \text{ p.u.} \quad (31)$$

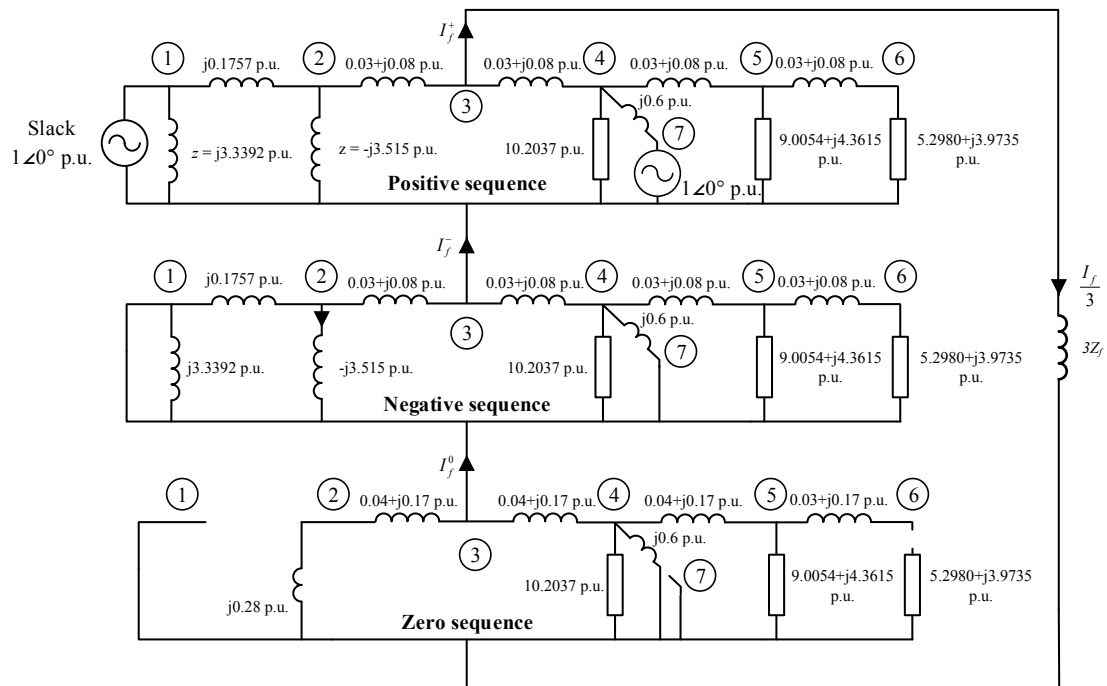


Figure 9. Sequence network of the test system (all values are in p.u.).

This study calculated the SCC ( $I_f^+$ ) that flowed from the voltage source, as follows:

$$I_f^+ = \frac{V_f}{(Z_i^+ + Z_i^- + Z_i^0 + 3Z_f)} = 1.5200 \angle -82.92^\circ \text{ p.u.} \quad (32)$$

where

$V_f = 1.0 \angle 0^\circ$  p.u.,  $Z_i^+ = Z_i^- = 0.0255 + 0.1859j$  p.u.,  $Z_i^0 = 0.0301 + 0.2811j$  p.u.,  $i = 3$ , and  $Z_f = 0$ .

Table 2 shows the SCCs after an SLG fault has occurred on phase *a* of bus 3. The first column presents the SCC when using the proposed SCC model and the pre-fault voltage that was determined by the proposed power-flow calculation method. The second column indicates the SCC when ignoring the load, which could be seen as a conventional method that neglected the load currents. The third

column presents the SCC of the conventional method that replaced the load by the impedance, using the nominal voltage. The SCCs that were determined by the IEC 60909 and complete modes of DIgSILENT are also included in the fourth and fifth columns. To find the actual SCC, this study calculated the power flow of the test system, using DIgSILENT. Table 3 indicates the unbalanced power-flow results. Then, this study superimposed the SCC that ignored the loads on the load currents that were determined by DIgSILENT, based on Equation (15).

$$\begin{aligned} I_{fault} &= I_{f,no-load} + I_{load,phase a} \\ &= 4.4890\angle -85.10^\circ + 0.2125\angle -30.59^\circ = 4.6156\angle -82.95^\circ \text{ p.u.} \end{aligned} \quad (33)$$

Table 4 compares the average of absolute errors (AEs) for all of the fault types. In Tables 2 and 4, the proposed method shows the closest match to the actual value (e.g., an AE of 1.20% for an SLG fault and an averaging AE of 1.68% for all of the fault types). Moreover, it was closer to the results of DIgSILENT than the conventional methods were. The detailed results of the other fault types (e.g., LLG, LL, and 3-phase faults) are presented in the Appendix A. Since the proposed method presented the lowest average of AEs (e.g., 1.68% in Table 4), it was more accurate than the conventional methods for calculating the SCC.

**Table 2.** Short-circuit current (SCC) (single line-to-ground [SLG] fault on bus 3); AE—absolute error; V—voltage.

Phase	Proposed Method	No Load (Conventional)	Load Replaced by Impedance( $V_{nom}$ )	DIgSILENT		Superposition (Actual)
	p.u.	p.u.	p.u.	IEC60909	Complete Mode	p.u.
<i>a</i>	$4.5600\angle -82.92^\circ$	$4.4890\angle -85.10^\circ$	$4.5354\angle -83.23^\circ$	$4.9375\angle -85.10^\circ$	$4.7366\angle -116.90^\circ$	$4.6156\angle -82.95^\circ$
AE	1.20%	2.74%	1.74%	6.97%	2.62%	-

**Table 3.** Unbalanced power-flow results calculated by DIgSILENT (generation, voltage, and current in p.u.).

Bus		Phase <i>a</i>	Phase <i>b</i>	Phase <i>c</i>	Total
1	Voltage	$1.000\angle 0.00^\circ$	$1.000\angle -120.00^\circ$	$1.000\angle 120.00^\circ$	-
	Generation	$0.096 + 0.038j$	$0.031 + 0.075j$	$0.032 + 0.001j$	$0.159 + 0.114j$
2	Voltage	$1.053\angle -32.14^\circ$	$1.014\angle -152.22^\circ$	$1.033\angle 89.71^\circ$	-
	Current ( $I_{load}$ )	$0.2125\angle -30.59^\circ$	$0.3019\angle 164.68^\circ$	$0.1119\angle 14.71^\circ$	-
3	Voltage	$1.047\angle -33.08^\circ$	$0.991\angle -152.88^\circ$	$1.023\angle 89.76^\circ$	-
4	Voltage	$1.042\angle -34.03^\circ$	$0.968\angle -153.58^\circ$	$1.014\angle 89.81^\circ$	-
5	Voltage	$1.040\angle -33.47^\circ$	$0.930\angle -155.12^\circ$	$1.015\angle 89.55^\circ$	-
6	Voltage	$1.040\angle -33.47^\circ$	$0.927\angle -155.57^\circ$	$1.007\angle 89.54^\circ$	-
7	Voltage	$1.000\angle -60.00^\circ$	$1.000\angle 180.00^\circ$	$1.000\angle 60.00^\circ$	-
	Generation	$0.017 - 0.026j$	$0.049 + 0.001j$	$0.010 + 0.015j$	$0.076 - 0.010j$

**Table 4.** Average of absolute error (AE) of each method to the actual SCC.

Method	The Proposed Method	No Load (Conventional)	Load Replaced by Impedance ( $V_{nom}$ )
Average of AE in %	1.68%	3.59%	2.46%

To validate the proposed methods, this study also changed the capacity of the loads from 0 p.u. to infinity, when an SLG fault occurred on phase *a* of bus 3. If the load capacity was set to zero, its equivalent impedance was an open circuit, and an SCC of  $4.4890\angle-85.10^\circ$  p.u. flowed to the ground, which corresponded to the case that ignored the loads, as shown in Table 2. If the load capacity increased up to infinity, its equivalent impedance (e.g.,  $Z = V^2/\infty = 0$ ) was a short circuit so that a large SCC of  $11.3873\angle-72.85^\circ$  p.u. could flow to the ground (Figure 10).

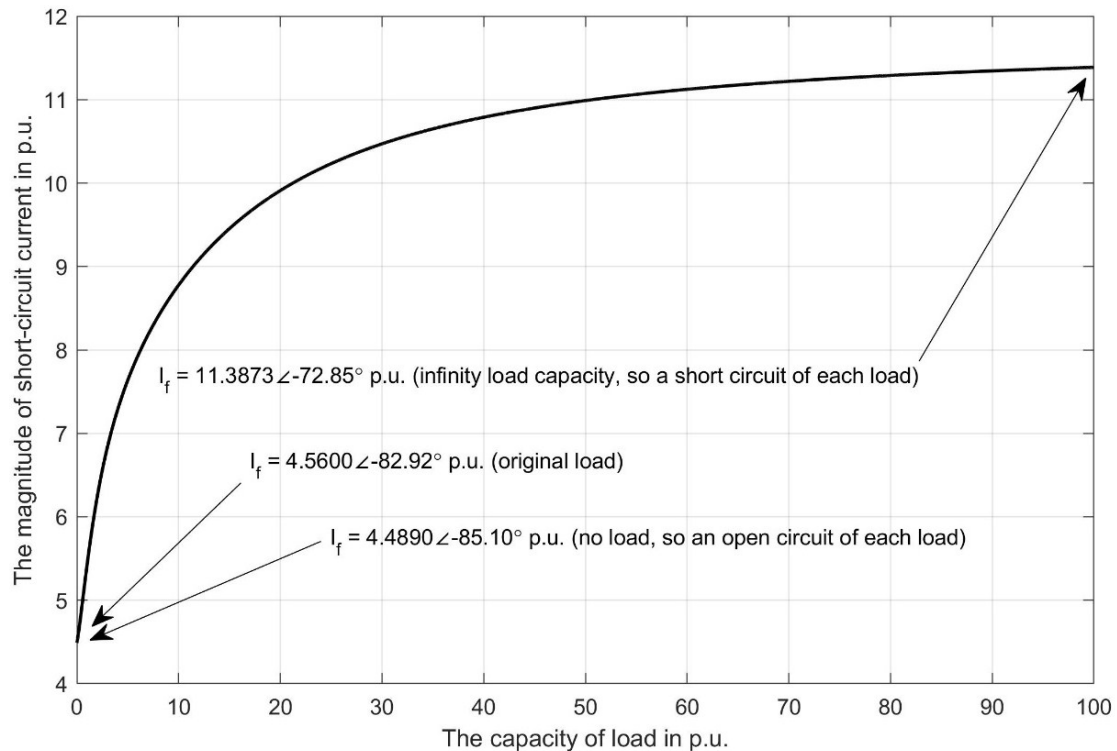


**Figure 10.** Magnitude of the single line-to-ground (SLG) fault current when changing the load capacity.

#### 4.2. Heavily-Meshed Network

To verify the proposed methods in a heavily-meshed network, the IEEE 30-bus test system was modeled, which was a power system network that was presented from American Electric Power in December 1961 [33,34], in Figure 11. It included 30 buses, a slack generator (represented as a slack bus on bus 1), five generators (represented as a P-V bus on buses 2, 5, 8, 11, and 13), two shunt capacitors, and 21 loads. To verify the proposed short-circuit analysis method in such a heavily-meshed network, the following conditions were assumed.

- (1) Since the zero-sequence impedance data of the system was not available, they were set to as much as 2.75 times the corresponding positive-sequence impedance data [35].
- (2) Since the detailed connection data of the transformers was not available, they were connected in a grounded wye-grounded wye configuration and all of the loads were unbalanced in a delta configuration.
- (3) All of the initial and target voltages of the generators were set to  $1.0\angle 0^\circ$  p.u., but it could have been specified differently, if necessary. The other data were set to the same data as was presented in [33], including the tap ratios of the tap-changing transformers and reactive power limits of the P-V buses.

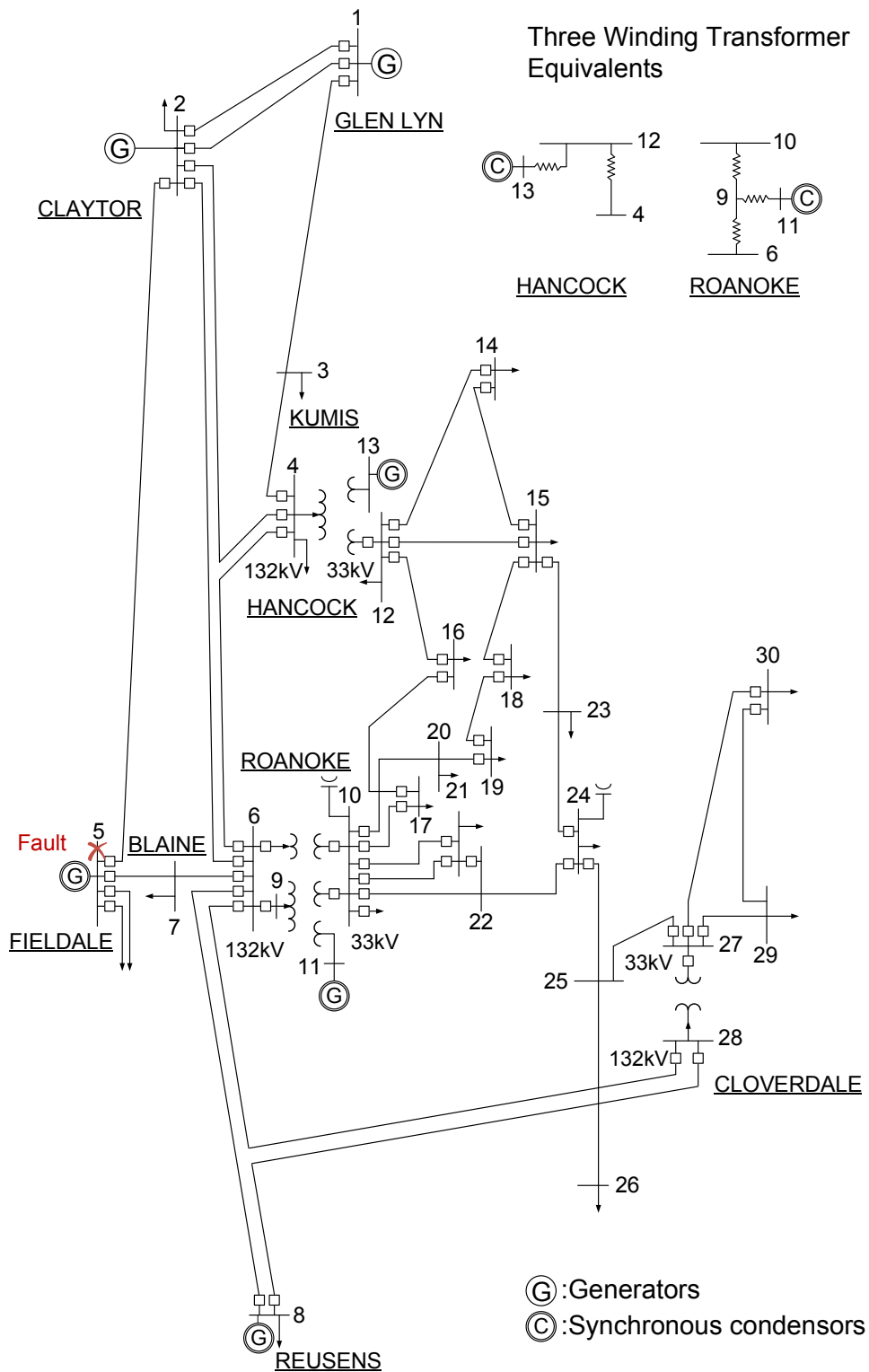


Figure 11. The heavily-meshed IEEE 30-bus test system [33,34].

The proposed power-flow method showed the same results as those that were calculated by the Gauss–Seidel, Newton–Raphson, and fast decoupled methods, which are presented in the Appendix A. Then, this study generated an SLG fault on bus 5. In order to take the effect of the unbalanced loads on the SCC into account, this study calculated the pre-fault voltage by the proposed power-flow algorithm, transformed the loads to the equivalent impedances, and added them to the sequence

networks. For example, the load with a capacity of  $21.7 + 12.7j$  MVA that was connected to bus 2 was transformed by the following:

$$Z_{B2}^{\Delta} = \frac{V_{B2}^2}{3S_{B2}^*} = \frac{0.977819^2}{3(0.217 + 0.127j)^*} = 1.0940 + j0.6403 \text{ p.u.} \quad (34)$$

where

$V_{B2} = 0.977819 \angle -6.035^\circ$  p.u. in Table A3 in the Appendix A.

Then, this study calculated the SCC by the following:

$$I_f^+ = \frac{V_f}{(Z_i^+ + Z_i^- + Z_i^0 + 3Z_f)} = 1.4922 \angle -65.91^\circ \text{ p.u.} \quad (35)$$

where

$V_f = 1.0 \angle 0^\circ$  p.u.,  $Z_i^+ = Z_i^- = 0.0673 + j0.0853$  p.u.,  $Z_i^0 = 0.1389 + j0.4412$  p.u.,  $i = 5$ , and  $Z_f = 0$ . Table 5 shows the SCC if an SLG fault occurred on bus 5. The actual SCC was calculated by the superposition rule, based on Equation (15). The unbalanced loads increased the magnitude of the SCC, compared with the method that ignored loads (e.g., the conventional method). It was because the unbalanced load conditions could decrease the impedance that was seen from the faulted bus by adding the SCC models of the unbalanced loads. Thus, as either the distributed or clustered loads that were unbalanced in phases were connected to the grid, the phase angle and magnitude of the SCC should have been accurately calculated. In other words, the loads should have been taken into account.

**Table 5.** SCC (SLG fault on bus 5).

Phase	Proposed Method	Conventional	Actual
<i>a</i>	$4.4760 \angle -65.91^\circ$ p.u.	$3.8076 \angle -72.78^\circ$ p.u.	$4.2370 \angle -59.32^\circ$ p.u.
AE	5.64%	10.13%	-

As the next validation step, this study presented the magnitude of the SCC when changing the faulted bus from buses 2 to 30, in Figure 12. For example, if an SLG fault occurred on phase *a* of bus 2, close to the slack generator (e.g., bus 1), the highest SCC of  $12.4659 \angle -69.71^\circ$  p.u. would flow. On the other hand, if the fault occurred on the bus (e.g., bus 26) that was remote from the slack generator, the lowest SCC of  $0.7160 \angle -62.62^\circ$  p.u. would flow, which was comparable to [27,28,36]. That is, as an SLG fault occurred closer to the slack generator, the higher SCC would flow. Figure 13a,b show a surface map and a contour map of all of the bus voltages when the fault location was changed from buses 2 to 30. In Figure 13a,b, if an SLG fault occurred on phase *a* of bus 2, the post-fault voltage magnitudes of the slack bus (e.g., bus 1) and the faulted bus (e.g., bus 2) indicated 1.0 p.u. and 0 p.u., respectively. The voltage magnitudes of the buses behind the faulted bus also showed about 0 p.u. If the fault occurred on bus 30, the voltage magnitudes of the slack bus (e.g., bus 1) and the faulted bus (e.g., bus 30) showed 1.0 p.u. and 0 p.u., respectively. In Figure 13b, the phase voltage of the faulted bus was 0 p.u. after an SLG fault. In the contour map, the phase voltage magnitude of 0 p.u. of each faulted bus changed diagonally, as the faulted bus was changed from 2 to 30.

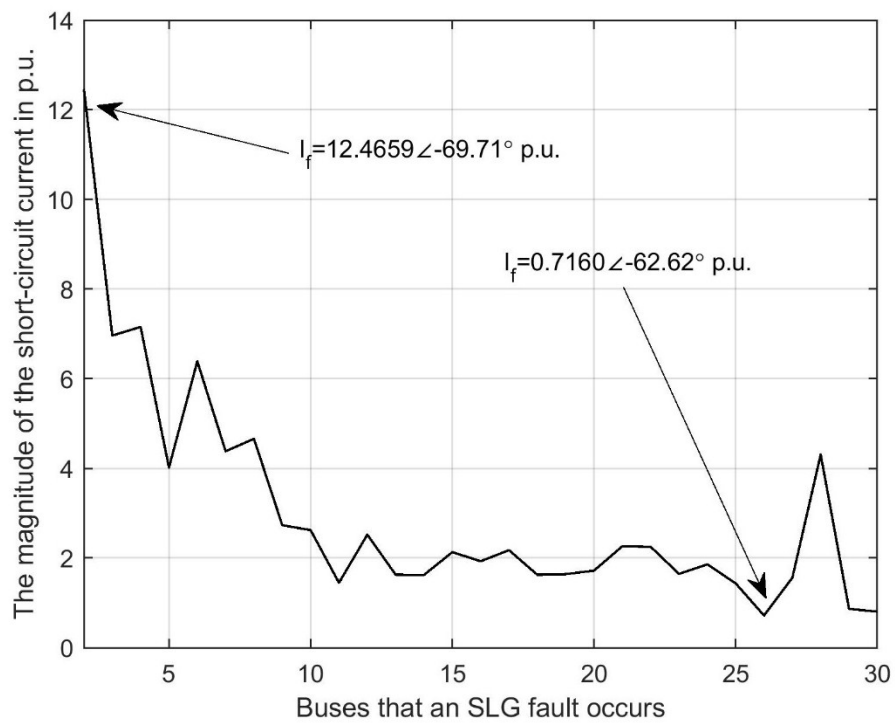


**Figure 12.** The magnitude of the short-circuit current (SCC) when changing the faulted location from buses 2 to 30.

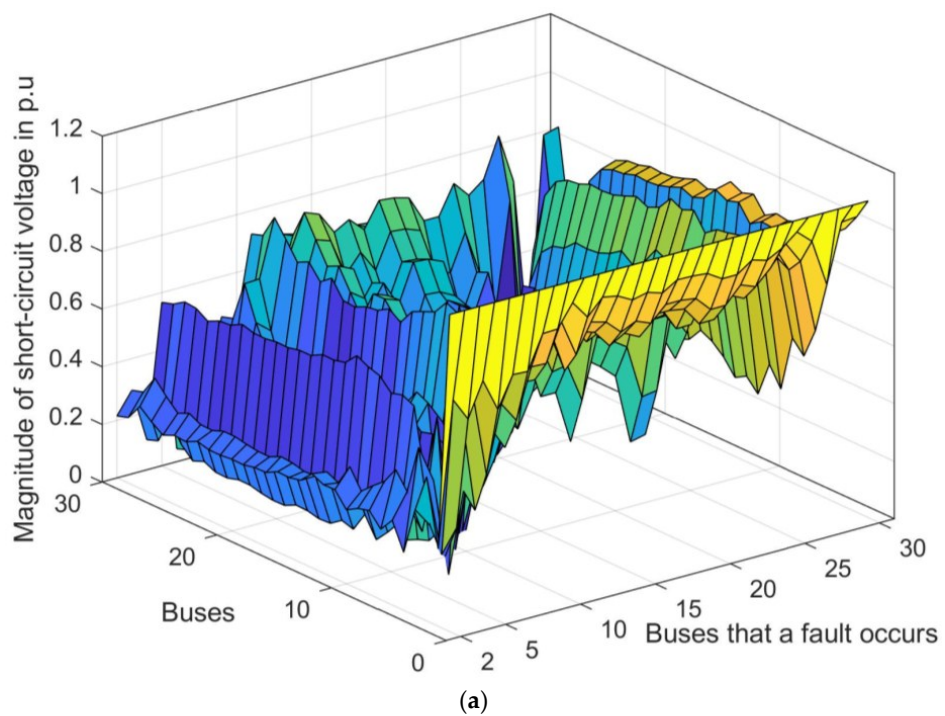


**Figure 13.** Cont.

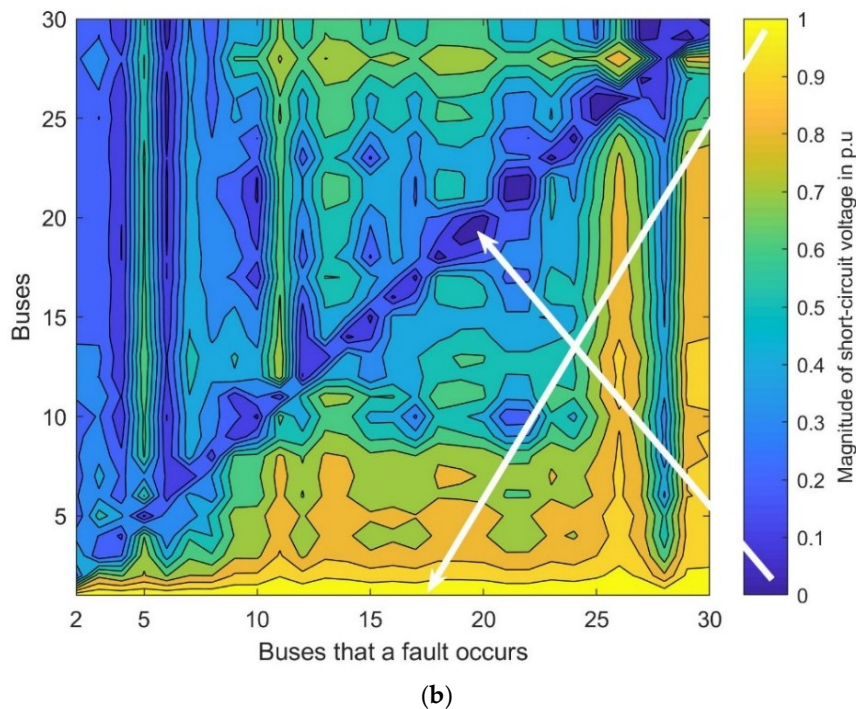


**Figure 13.** The magnitude of voltage of phase *a* when an SLG fault occurs on phase *a* of buses from 2 to 30: (a) surface map and (b) contour map.

## 5. Conclusions

The main objective of this study is to present a short-circuit analysis algorithm that is able to analyze unbalanced loads. For this purpose, this study derives an SCC model of the unbalanced wye- or delta-connected impedance load. Since the proposed SCC model requires the pre-fault voltage, it uses a power-flow analysis algorithm that iteratively calculates the current that needs to be injected and the pre-fault voltage, using the bus impedance matrix. The case studies of the unbalanced test feeders indicate that the proposed SCC model, which transforms the unbalanced loads to the equivalent short-circuit impedances, shows the least AEs to the actual SCC, compared with the conventional methods. In other words, the proposed short-circuit analysis method could more accurately calculate the SCC, since it did not neglect the unbalanced loads. Thus, the proposed short-circuit method is able to take the unbalanced wye- or delta-connected loads into account.

The proposed SCC model is based on an unbalanced load, so it is applicable to the unbalanced systems. The proposed SCC models are also applicable for the cases either with or without DG. Since the proposed SCC models are more accurate than the conventional methods that neglect the load, the proposed SCC models of delta- or wye-connected unbalanced loads in phases can be incorporated in the power systems analysis programs (e.g., DIGSILENT). However, this study did not examine the effect of unbalanced loads with various capacities that have uncertainty in their capacity and location on the SCC. In addition to the uncertainty, it did not present a method that transforms constant current and power loads into equivalent short-circuit impedance. Implementing these topics in future should provide a more accurate method for short-circuit studies.

**Funding:** This work was supported by the Inha University Research Grant #57843-1.

**Conflicts of Interest:** The authors declare no conflict of interest.

## Nomenclature

AE	absolute error
BIBC	bus-current-injection to branch-current
BCBV	branch-current to bus-voltage
BFSW	backward and forward Sweep
DG	distributed generation
IBDG	inverter based distributed generation
LLG	line-to-line ground
LL	line-to-line
KCL	Kirchhoff's Current Law
PF	power factor
p.u.	per unit
S	complex power
SCC	short-circuit current
SLG	single line-to-ground
V	voltage
$V_f$	faulted bus voltage
Z	impedance
$Z_{bus}$	bus impedance matrix

## Appendix A

### Appendix A.1. Short-Circuit Current

Table A1 shows the SCC of each sequence network for SLG, LLG, LL, and 3-phase faults.

**Table A1.** Fault current of each sequence network [37].

Type	Positive-Sequence ( $I_i^+$ )	Negative-Sequence ( $I_i^-$ )	Zero-Sequence ( $I_i^0$ )
SLG	$\frac{V_f}{(Z_i^+ + Z_i^- + Z_i^0 + 3Z_f)}$	$\frac{V_f}{(Z_i^+ + Z_i^- + Z_i^0 + 3Z_f)}$	$\frac{V_f}{(Z_i^+ + Z_i^- + Z_i^0 + 3Z_f)}$
LLG	$\frac{V_f}{Z_i^-    ((Z_i^0 + 3Z_f) + Z_i^+)}$	$-\frac{Z_i^0 + 3Z_f}{Z_i^- + Z_i^0 + 3Z_f} I_i^+$	$-\frac{Z_i^-}{Z_i^- + Z_i^0 + 3Z_f} I_i^+$
LL	$\frac{V_f}{(Z_i^+ + Z_i^- + Z_f)}$	$-\frac{V_f}{(Z_i^+ + Z_i^- + Z_f)}$	0
3-phase	$\frac{V_f}{(Z_f + Z_i^+)}$	0	0

where  $V_f$  = the Thevenin voltage source, typically  $1.0 \angle 0^\circ$  p.u.,  $Z_i^+$ ,  $Z_i^-$ , and  $Z_i^0$  = the  $i$ th diagonal element of each bus impedance matrix,  $Z_f$  = the short-circuit impedance.

### Appendix A.2. Other Fault Types

Table A2 shows the SCCs for the SLG, LLG, LL, and 3-phase faults of the seven-bus radial system. Expectedly, the magnitude of the 3-phase SCC is the highest. The proposed method indicates the least AEs to the actual SCC, is determined by the superposition rule based on (15).

**Table A2.** SCC in p.u. (fault on bus 3).

Ph	The proposed method that uses the pre-fault voltage determined by the proposed power-flow calculation method								Average AE
	SLG		LLG		LL		3-Phase		
	p.u.	AE in %	p.u.	AE in %	p.u.	AE in %	p.u.	AE in %	
a	4.5600 $\angle -82.92^\circ$	1.20%	-	-	-	-	5.3292 $\angle -82.20^\circ$	0.27%	1.68%
b	-	-	4.9861 $\angle 164.26^\circ$	4.20%	4.6152 $\angle -172.20^\circ$	3.87%	5.3292 $\angle 157.80^\circ$	3.36%	
c	-	-	5.0672 $\angle 30.95^\circ$	0.11%	4.6152 $\angle 7.80^\circ$	0.27%	5.3292 $\angle 37.80^\circ$	0.15%	

Table A2. Cont.

The conventional method that the load is replaced by impedance using the nominal voltage									
<i>a</i>	4.5354∠−83.23°	1.74%	-	-	-	-	5.2794∠−82.76°	1.21%	
<i>b</i>	-	-	4.9589∠163.62°	4.73%	4.5721∠−172.76°	4.77%	5.2794∠157.24°	4.26%	2.46%
<i>c</i>	-	-	5.0118∠30.60°	0.98%	4.5721∠7.24°	1.21%	5.2794∠37.24°	0.78%	
The conventional method that the load is ignored									
<i>a</i>	4.4890∠−85.10°	2.74%	-	-	-	-	5.2163∠−84.65°	2.39%	
<i>b</i>	-	-	4.9034∠161.67°	5.79%	4.5175∠−174.65°	5.91%	5.2163∠155.35°	5.41%	3.59%
<i>c</i>	-	-	4.9529∠28.78°	2.15%	4.5175∠5.35°	2.39%	5.2163∠35.35°	1.97%	
The actual SCC based on the superposition rule									
<i>a</i>	4.6156∠−82.95°		-		-		5.3438∠−82.80°		
<i>b</i>	-		5.2049∠161.84°		4.8011∠−175.92°		5.5145∠155.86°		-
<i>c</i>	-		5.0615∠28.48°		4.6279∠5.58°		5.3211∠34.93°		

### Appendix A.3. Power-Flow Solutions of the IEEE 30-Bus Test System

The power-flow solutions of the IEEE 30-bus test system, calculated by the proposed method, show the same results as those that are calculated by the Gauss–Seidel, Newton–Raphson, and fast decoupled methods. Note that the reactive power limits of the P-V buses are set to the same data as presented in [33].

Table A3. Positive-sequence pre-fault voltage of the IEEE 30-bus test system in p.u.

Bus	Type	Proposed Method ( $Z_{bus}$ )	Newton–Raphson Method ( $Y_{bus}$ )	Gauss–Seidel Method ( $Y_{bus}$ )	Fast Decoupled Method ( $Y_{bus}$ )
1	Slack	1.000000∠0.000°	1.000000∠0.000°	1.000000∠0.000°	1.000000∠0.000°
2	P-V	0.977819∠−6.035°	0.977819∠−6.035°	0.977819∠−6.035°	0.977819∠−6.035°
3	P-Q	0.952382∠−8.516°	0.952382∠−8.516°	0.952382∠−8.516°	0.952382∠−8.516°
4	P-Q	0.941965∠−10.520°	0.941965∠−10.520°	0.941965∠−10.520°	0.941965∠−10.520°
5	P-V	0.942303∠−16.185°	0.942303∠−16.185°	0.942303∠−16.185°	0.942303∠−16.185°
6	P-Q	0.939358∠−12.555°	0.939358∠−12.555°	0.939358∠−12.555°	0.939358∠−12.555°
7	P-Q	0.932001∠−14.651°	0.932001∠−14.651°	0.932002∠−14.651°	0.932001∠−14.651°
8	P-V	0.939909∠−13.436°	0.939909∠−13.436°	0.939909∠−13.436°	0.939909∠−13.436°
9	P-Q	0.972063∠−16.077°	0.972063∠−16.077°	0.972063∠−16.077°	0.972063∠−16.077°
10	P-Q	0.964874∠−17.931°	0.964874∠−17.931°	0.964874∠−17.931°	0.964874∠−17.931°
11	P-V	1.000000∠−16.077°	1.000000∠−16.077°	1.000000∠−16.077°	1.000000∠−16.077°
12	P-Q	0.981403∠−17.112°	0.981403∠−17.112°	0.981403∠−17.112°	0.981403∠−17.112°
13	P-V	1.000000∠−17.112°	1.000000∠−17.112°	1.000000∠−17.112°	1.000000∠−17.112°
14	P-Q	0.964859∠−18.147°	0.964859∠−18.147°	0.964859∠−18.147°	0.964859∠−18.147°
15	P-Q	0.959434∠−18.240°	0.959434∠−18.240°	0.959434∠−18.240°	0.959434∠−18.240°
16	P-Q	0.966131∠−17.756°	0.966131∠−17.756°	0.966131∠−17.756°	0.966131∠−17.756°
17	P-Q	0.959843∠−18.132°	0.959843∠−18.132°	0.959843∠−18.132°	0.959843∠−18.132°
18	P-Q	0.948151∠−18.946°	0.948151∠−18.946°	0.948151∠−18.946°	0.948151∠−18.946°
19	P-Q	0.944882∠−19.142°	0.944882∠−19.142°	0.944882∠−19.142°	0.944882∠−19.142°
20	P-Q	0.949026∠−18.905°	0.949026∠−18.905°	0.949026∠−18.905°	0.949026∠−18.905°
21	P-Q	0.951519∠−18.450°	0.951519∠−18.450°	0.951519∠−18.450°	0.951519∠−18.450°
22	P-Q	0.952130∠−18.433°	0.952130∠−18.433°	0.952130∠−18.433°	0.952130∠−18.433°
23	P-Q	0.947173∠−18.680°	0.947173∠−18.680°	0.947173∠−18.680°	0.947173∠−18.680°
24	P-Q	0.939936∠−18.863°	0.939936∠−18.863°	0.939936∠−18.863°	0.939936∠−18.863°
25	P-Q	0.937200∠−18.400°	0.937200∠−18.400°	0.937201∠−18.400°	0.937200∠−18.400°
26	P-Q	0.917944∠−18.896°	0.917944∠−18.896°	0.917944∠−18.896°	0.917944∠−18.896°
27	P-Q	0.944837∠−17.806°	0.944837∠−17.806°	0.944837∠−17.806°	0.944837∠−17.806°
28	P-Q	0.935192∠−13.274°	0.935192∠−13.274°	0.935192∠−13.274°	0.935192∠−13.274°
29	P-Q	0.923146∠−19.254°	0.923146∠−19.254°	0.923146∠−19.254°	0.923146∠−19.254°
30	P-Q	0.910609∠−20.299°	0.910609∠−20.299°	0.910609∠−20.299°	0.910609∠−20.299°

## References

1. Zhou, N.; Wu, J.; Wang, Q. Three-phase short-circuit current calculation of power systems with high penetration of VSC-based renewable energy. *Energies* **2018**, *11*, 537. [[CrossRef](#)]
2. Gross, G.; Hong, H.W. A two-step compensation method for solving short circuit problems. *IEEE Trans. Power Appl. Syst.* **1982**, *101*, 1322–1331. [[CrossRef](#)]
3. Kersting, W.H. *Distribution System Modeling and Analysis*; CRC Press: Boca Raton, FL, USA, 2002.
4. Bordalo, U.A.; Rodrigues, A.B.; Silva, M.G.D. A new methodology for probabilistic short-circuit evaluation with applications in power quality analysis. *IEEE Trans. Power Syst.* **2006**, *21*, 474–479. [[CrossRef](#)]
5. Teng, J.H. Unsymmetrical short-circuit fault analysis for weakly meshed distribution systems. *IEEE Trans. Power Syst.* **2010**, *25*, 96–105. [[CrossRef](#)]
6. Chen, T.; Chen, M.; Lee, W.; Kotas, P.; van Olinda, P. Distribution system short circuit analysis—A rigid approach. *IEEE Trans. Power Syst.* **1992**, *7*, 444–450. [[CrossRef](#)]
7. Zhang, X.; Soudi, F.; Shirmohammadi, D.; Cheng, C.S. A distribution short circuit analysis approach using hybrid compensation method. *IEEE Trans. Power Syst.* **1995**, *10*, 2053–2059. [[CrossRef](#)]
8. Abdel-Akher, M.; Nor, K.M. Fault analysis of multiphase distribution systems using symmetrical components. *IEEE Trans. Power Deliv.* **2010**, *25*, 2931–2939. [[CrossRef](#)]
9. Fan, C.; Liu, L.; Tian, Y. A fault-location method for 12-phase transmission lines based on twelve-sequence-component method. *IEEE Trans. Power Deliv.* **2011**, *26*, 135–142. [[CrossRef](#)]
10. Gajbhiye, R.K.; Kulkarni, P.; Soman, S.A. Analysis of faulted power systems in three phase coordinates—A generic approach. In Proceedings of the 7th International Power Engineering Conference, Singapore, 29 November–2 December 2005.
11. Penido, D.R.R.; de Araujo, L.R.; Júnior, S.C.; Pereira, J.L.R. A new tool for multiphase electrical systems analysis based on current injection method. *Int. J. Electr. Power Energy Syst.* **2013**, *44*, 410–420. [[CrossRef](#)]
12. Penido, D.R.R.; de Araujo, L.R.; Filho, M.D. An enhanced tool for fault analysis in multiphase electrical systems. *Int. J. Electr. Power Energy Syst.* **2016**, *75*, 215–225. [[CrossRef](#)]
13. Lacroix, J.S.; Kocar, I.; Belletête, M. Accelerated computation of multiphase short circuit summary for unbalanced distribution systems using the concept of selected inversion. *IEEE Trans. Power Syst.* **2013**, *28*, 1515–1522. [[CrossRef](#)]
14. Youssef, K.H.; Abouelenin, F.M. Analysis of simultaneous unbalanced short circuit and open conductor faults in power systems with untransposed lines and six-phase sections. *Alex. Eng. J.* **2016**, *55*, 369–377. [[CrossRef](#)]
15. Laughton, M.A. Analysis of unbalanced polyphase networks by the method of phase co-ordinates, Part 2 Fault analysis. *Proc. Inst. Electr. Eng.* **1969**, *116*, 5. [[CrossRef](#)]
16. Bai, X.; Jiang, T.; Guo, Z.; Yan, Z.; Ni, Y. A unified approach for processing unbalanced conditions in transient stability calculations. *IEEE Trans. Power Syst.* **2006**, *21*, 85–90. [[CrossRef](#)]
17. Mathur, A.; Das, B.; Pant, V. Fault analysis of unbalanced radial and meshed distribution system with inverter based distributed generation (IBDG). *Int. J. Electr. Power Energy Syst.* **2017**, *85*, 164–177. [[CrossRef](#)]
18. Ou, T. A novel unsymmetrical faults analysis for microgrid distribution systems. *Int. J. Electr. Power Energy Syst.* **2012**, *43*, 1017–1024. [[CrossRef](#)]
19. Filomena, A.D.; Resener, M.; Salim, R.H.; Bretas, A.S. Distribution systems fault analysis considering fault resistance estimation. *Int. J. Electr. Power Energy Syst.* **2011**, *33*, 1326–1335. [[CrossRef](#)]
20. Gross, C.A. *Power System Analysis*; Wiley: New York, NY, USA, 2013; pp. 357–359.
21. Eslami, A. A three-phase comprehensive methodology to analyze short circuits, open circuits and internal faults of transformers based on the compensation theorem. *Int. J. Electr. Power Energy Syst.* **2018**, *96*, 238–252. [[CrossRef](#)]
22. Mathur, A.; Pant, V.; Das, B. Unsymmetrical short-circuit analysis for distribution system considering loads. *Int. J. Electr. Power Energy Syst.* **2015**, *70*, 27–38. [[CrossRef](#)]
23. Verma, S.C.; Nakachi, Y.; Wazawa, Y.; Kosaka, Y.; Kobayashi, T.; Omata, K.; Takabayashi, Y. Short circuit current estimation using PMU measurements during normal load variation. In Proceedings of the 2012 3rd IEEE PES Innovative Smart Grid Technologies Europe, Berlin, Germany, 14–17 October 2012.

24. Pan, R.; Liu, J.; Wang, M.; Liu, Y.; Hou, H. Ultra-real time short circuit current computing based on ultra-short term load forecasting. In Proceedings of the 2010 Asia-Pacific Power and Energy Engineering Conference, Chengdu, China, 28–31 March 2010.
25. Ge, J.T.; Cao, W.; Ding, Z.G.; Yu, Y. Short-circuit current calculation approach with dynamic load considered in PSS/E short circuit portion. In Proceedings of the IEEE PES Innovative Smart Grid Technologies, Tianjin, China, 12–24 May 2012.
26. Cao, W.; Liu, B.; Wang, W. The impact of dynamic load on 3-phase short-circuit current of metropolitan transmission network. In Proceedings of the 2011 Asia-Pacific Power and Energy Engineering Conference, Wuhan, China, 25–28 March 2011.
27. Kim, I. The effect of load current on a three-phase fault. In Proceedings of the Seventh Conference on Innovative Smart Grid Technologies, Minneapolis, MN, USA, 6–9 September 2016.
28. Kim, I.; Harley, R.G. A study on power-flow and short-circuit algorithms capable of analyzing the effect of load current on fault current using the bus impedance matrix. In Proceedings of the 2016 Electrical Power and Energy Conference, Ottawa, ON, Canada, 12–14 October 2016.
29. CYME International. *CYME 7.2—Fault Analysis—Users Guide*; CYME International: Québec, QC, Canada, 2015; p. 9.
30. DIgSILENT GmbH. *DIgSILENT Power Factory Reference Manual*; Technical Report; DIgSILENT GmbH: Gomaringen, Germany, 2015.
31. Teng, J. A direct approach for distribution system load flow solutions. *IEEE Trans. Power Deliv.* **2003**, *18*, 882–887. [[CrossRef](#)]
32. Brown, H.E.; Carter, G.K.; Happ, H.H.; Person, C.E. Power flow solution by impedance matrix iterative method. *IEEE Trans. Power Appl. Syst.* **1963**, *82*, 1–10. [[CrossRef](#)]
33. Dabbagchi, I. IEEE 30-Bus System, American Electric Power System. Available online: [www.ee.washington.edu/research/pstca/pf30/pg\\_tca30bus.htm](http://www.ee.washington.edu/research/pstca/pf30/pg_tca30bus.htm) (accessed on 22 March 2018).
34. Working Group on A Common Format for Exchange of Solved Load Flow Data. Common format for exchange of solved load flow data. *IEEE Trans. Power App. Syst.* **1973**, *92*, 1916–1925.
35. Nagrath, K. *Power System Engineering*; Tata McGraw-Hill: New York, NY, USA, 2008.
36. Kim, I.; Harley, R.G. A study on the effect of distributed generation on short-circuit current. In Proceedings of the Power Systems Conference 2016, Clemson University, Clemson, SC, USA, 8–11 March 2016.
37. Glover, J.D.; Sarma, M.; Overbye, T. *Power System Analysis and Design*; Cengage Learning: Boston, MA, USA, 2011.



© 2018 by the author. Licensee MDPI, Basel, Switzerland. This article is an open access article distributed under the terms and conditions of the Creative Commons Attribution (CC BY) license (<http://creativecommons.org/licenses/by/4.0/>).